ATLAS PUB Note

September 11, 2017

Pileup noise behavior and corrections in the ATLAS EMCal

Jordan Seneca

Supervisor: Ludovica Aperio Bella, Guillaume Unal

In this note, the pile-up influence on the energy resolution of the ATLAS LAr EMCal expected until the end of run 2 is explored, with the supercluster algorithm. The pile-up noise is extracted for various η-regions and electron energies, and found to match the expected behavior. An attempt is then made at improving the energy resolution using the ambient energy density and pileup tracks using two methods for finding correlations. The corrections yield no significant improvement to the energy resolution due to small correlations.

1 Introduction

The Large Hadron Collider will be undergoing several phases of upgrade to increase its luminosity (HL-LHC). The increase in luminosity is achieved by an increase in pile-up at each bunch crossing [1]. Pile-up causes noise in the instruments of ATLAS. The purpose of this note is to characterize the effect of this pile-up on the energy reconstruction of the ATLAS Electromagnetic Calorimeter (EMCal).

The EMCal is a Liquid Argon (LAr) sampling calorimeter[2], and is the second instrument particles traverse after exiting the Inner Detector Tracking System (IDTS). The EMCal is composed of two main sections: the barrel (EMB) at pseudo-rapidity $|\eta|$ from 0 to 1.475, and two end caps (EMEC) at $|\eta|$ from 1.375 to 3.2. These sections are composed of three layers segmented in the longitudinal direction, and a pre-sampler closest to the IDTS in the region $|\eta| < 1.8$. The region $1.37 < \eta < 1.52$ is the transition region and suffers from worse energy estimation due to a large amount of material before the first active calorimeter layer.

The energy resolution in the EMCal is defined by Eqn.1:

$$\frac{\sigma_E}{E} = \frac{a}{\sqrt{E}} \oplus \frac{b}{E} \oplus c \tag{1}$$

Where $\frac{\sigma_E}{E}$ is the overall relative error on energy estimation. a is called the sampling term, b the noise term, and c the constant term. a is due to the structure of the LAr sampling calorimeter; a Poissonian fluctuation is introduced by secondary electrons produced in the insensitive gaps of the EMCal. b contains the fluctuation due to the noise from readout electronics and pile-up events. c is due to imperfections of the detector, such as impurities in the active medium or non-uniform thicknesses in the gaps.

The noise term b can be decomposed into its contributions from electronic noise and pileup noise:

$$b = \sigma_{pileup} \oplus \sigma_{electronic} \tag{2}$$

The pileup noise is in turn expected to experience a dependence on the average number of interactions per bunch crossings, μ, see Eqn.3.

$$\frac{\sigma_{pileup}}{E_t} = \beta(\eta, E_t)\sqrt{\mu} \oplus \alpha \tag{3}$$

Where β is the pileup noise factor and represents the pileup noise σ_{pileup} per $\sqrt{\mu}$ in E_t. β is expected to have a small dependence on E_t and η due to the influence of cell shapes and electron energy on the supercluster size. For a fixed E_t and η, we can rearrange Eqn.1 to find a linear dependence to μ by confining all the constant terms, a, c, and α[1].

$$\left(\frac{\sigma_E}{E}(\mu)\right)^2 = \frac{\beta^2 \mu}{E_t^2} + Constants \tag{4}$$

Looking at specific bins in E_t and η, we can now analyze the dependence of the energy resolution on μ directly and probe the pileup noise factor β.

[1] Note that $E = E_t cosh(\eta)$, so in a fixed bin of η, E and E_t are simply related by a constant factor, which is absorbed in β^2

2 Methodology for pile-up noise extraction

A fully simulated sample[2] from the mc16a production campaign of 900k events was provided. The sample uses the new run 2 clustering algorithm[3]. The dataset contains a single electron sample and a flat distribution of $0 \leq \mu \leq 60$, representative of the average expected pile-up until the end of run 2. It contains information on the true electrons from the simulation and the reconstructed particles from the EMCal.

For each true and reconstructed electron, the angle difference $\Delta R = \sqrt{(\Delta\eta)^2 + (\Delta\phi)^2}$ is computed between their respective directions. For this study, only reconstructed electrons with $\Delta R < 0.05$ were kept. Among those, the reconstructed electron closest to the true electron was designated as the matched electron and used. The relative energy difference is then computed, defined as:

$$\frac{\Delta_E}{E} = \frac{E_{matched} - E_{true}}{E_{true}} \tag{5}$$

Where $E_{matched}$ is the energy of the best match electron, and E_{true} is the energy of the true electron. The distribution of $\frac{\Delta_E}{E}$ is Gaussian fitted, and the standard deviation defined as the energy resolution, σ_e.

This process is repeated for every μ, in bins of E_t and η. The bins used are the following:

- μ bins: 0, 10, 20, 30, 40, 50, 60
- $E_t(GeV)$ bins: 7, 15, 20, 30, 50, 80, 120, 2000
- η bins: 0, 0.8, 1.37, 1.6, 1.82, 2.47

For every bin in η and E_t, the dependence of σ_E^2 on μ is plotted and fitted to a linear function, $A + B \times \mu$, see Fig.1(a). From Eqn.4, A corresponds to the constants, while B corresponds to $\frac{\beta^2}{E_t^2}$. The pileup noise factor $\beta \equiv \sigma_{noise}$ is finally extracted using Eqn.6.

$$\beta = \sqrt{B} * E_t \tag{6}$$

3 Measurements of pileup noise factor

In Fig.1(a), the dependency of σ_E^2 on μ is comfortably fitted by a linear function. For the middle η bin at low E_t, the slope is $(31.4 \pm 3.8) \times 10^{-6}$, and at high E_t, $(0.62 \pm 0.02) \times 10^{-6}$; a good fit with errors of 12% and 3.2% respectively[4]. The pileup noise factor is now extracted using Eqn.6. The pileup noise factor was expected to have some dependence on the position η in the EMCal and on the E_t of the reconstructed event. In Fig.1(b), there is a clear positive dependence of σ_{noise} on E_t. A dependence of σ_{noise} on the

[2] Filename: mc16_13TeV.423000.ParticleGun_single_electron_egammaET.merge.AOD.e3566_s3113_r9397_r9315

[3] A new approach to reconstruct electromagnetic (EM) energy deposits in the ATLAS EM calorimeter is to be employed in the future version of the ATLAS software (Athena Rel. 21). This so called Super-Cluster approach, starts from topological clusters identified in the ATLAS calorimeter, which then can be potentially merged based on information provided by the ATLAS tracking detector. The expected electron and photon energy calibration performance using this approach is presented and compared with the previous so called fixed-window approach.[3]

[4] See Appendix for more linear fits

position of the event is also apparent, for example, the noise factor seems to be consistently lower in the EMEC than in the EMB over all E_t except in the last bins, where the most extreme η bin experiences an increase. One can also verify that the actual number of cells, which is supposed to cause the small β dependence on E_t, does indeed increase with increasing E_t, see Fig.2(a).

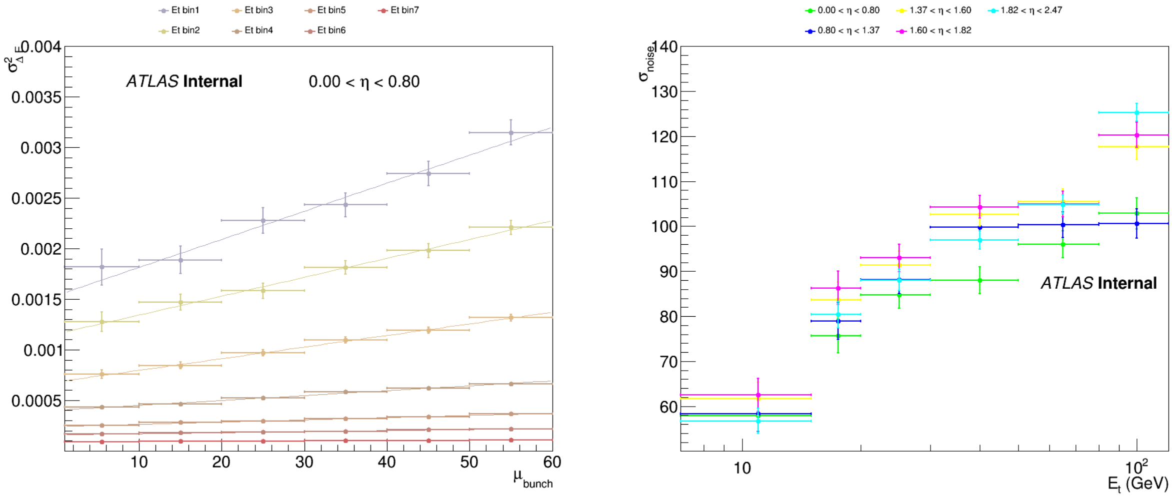

(a) Energy resolution squared vs. μ for all E_t bins in the first η bin of the barrel. Note the linear dependence of σ_E^2 on μ, as expected from Eqn.4. Both the intercept and the slopes are inversely proportional to E_t.

(b) σ_{noise} for every η and E_t bins (except last E_t bin).

Figure 1: All but last E_t bins for the $0 < |\eta| < 0.8$ EMB region.

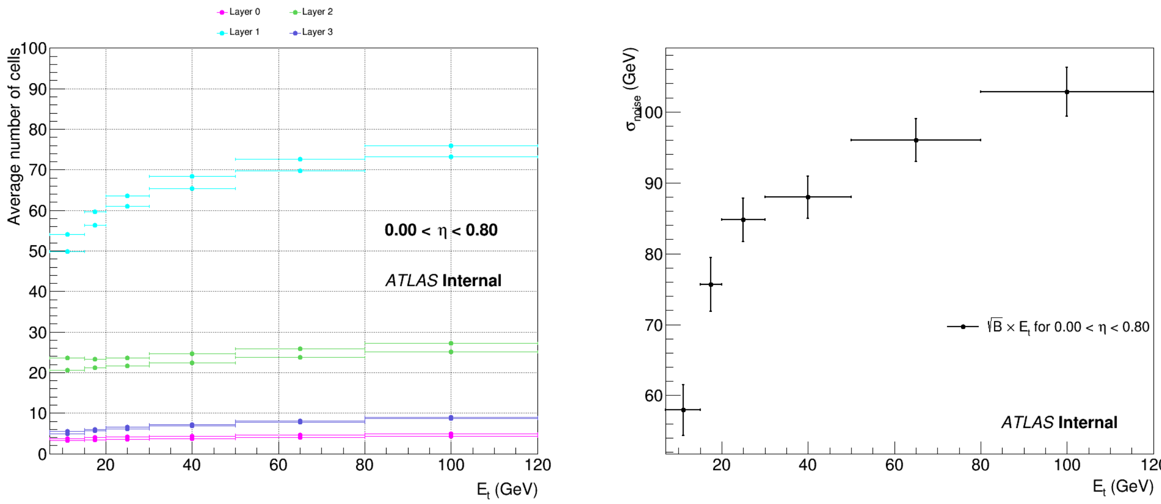

(a) Average number of cells in supercluster for each longitudinal layer in the EMB

(b) σ_{noise}

Figure 2: Effect of superclusters on pileup noise. Comparison for the $0 < |\eta| < 0.8$ EMB region. The increase in the number of cells in the supercluster results in a higher σ_{noise} at higher energies. The plots show that the dependency of the number of cells and σ_{noise} on E_t is closely related.

4 Methodology for correction of energy reconstruction

There are pileup related observables that are potentially correlated with the energy resolution of the EMcal. Three of these variables of interest (VOI) are explored in this study: The ambient energy density (ρ), the number of pileup matched tracks ($Ntracks$), and the cumulative energy of pileup matched tracks (Pt_{tracks}).

ρ has two components, ρ_{EMB} and ρ_{EMEC}, defined as the total energy in the two η regions of the calorimeter obtained from low E_t jets in TOPO clusters.

Pileup track information is introduced from the Inner Detector Tracking System (IDTS) of ATLAS. After finding the matched electron using the method described previously, the IDTS track of the matched electron is found. A selection is made of tracks that are present at DR > 0.04 with some quality requirements[5]. These tracks constitute our sample of pileup matched tracks, $tracks_{pileup}$. From these tracks, two pieces of information are used; their number, n_{tracks} and the sum of their momenta, Pt_{tracks}.

First, the three VOIs are found to have a strong linear dependence on μ, see Fig.12 and Fig.13. The expectation value of each initial VOI is found by taking its average value found at each μ.This information is then used to formulate three additional VOIs, $\Delta\rho \equiv \rho - <\rho>$, $\Delta n_{tracks} \equiv n_{tracks} - <n_{tracks}>$, and $\Delta Pt_{tracks} \equiv Pt_{tracks} - <Pt_{tracks}>$.

Next, the relation between each of our six VOIs and ΔE[6] is calculated. This is done using two methods. The first method uses the built in ROOT function TProfile which, at each value of the VOI, calculates the weighted average of ΔE. The second method finds, at each value of the VOI, the Gaussian fitted mean[7]. The means are linearly fitted, where the fit represent our correlations. This process is repeated for every η and E_t bins.

If a non negligible correlation is found between the VOI and ΔE, the Gaussian distribution of ΔE will be skewed across the full range of the VOI. We can then use the slope of the linear fit to correct for this dependence, resulting in a smaller total spread on ΔE, effectively improving the energy resolution on electron energy reconstruction.

Events from the sample are selected again, but this time, the value of the linear fit of the profile and Gaussian means at the VOI-value is subtracted from each $E_{matched}$ to correct for the dependence on the VOI. The result is the corrected distribution of ΔE using the VOI and profile and Gaussian methods.

5 Results of energy reconstruction corrections

None of the corrections were able to yield a consistent significant improvement on the error on ΔE across the E_t range, both using the Gaussian and profile corrections. Fig.3 shows the attempts at improving the energy resolution for the first EMB region using $\rho - <\rho>$. This is explained by very small albeit clear correlations of ΔE which yield negligible corrections, see Fig.4. The means of the distribution were accurately corrected, but the Gaussian corrections achieved better results than the profile corrections,

[5] Number of hits in the pixel detectors and semiconductor trackers > 4, $Pt < 10000 MeV$

[6] Note that we are using ΔE and not $\frac{\Delta E}{E}$ as before. The reason for this is that correlations are more apparent for the absolute energy difference.

[7] "Profile corrections" and "Gaussian corrections" will refer to these two respective methods

which had a tendency to overshoot the mean. A typical mean correction is shown in Fig.17(b), using n_{tracks} in the first EMEC region.

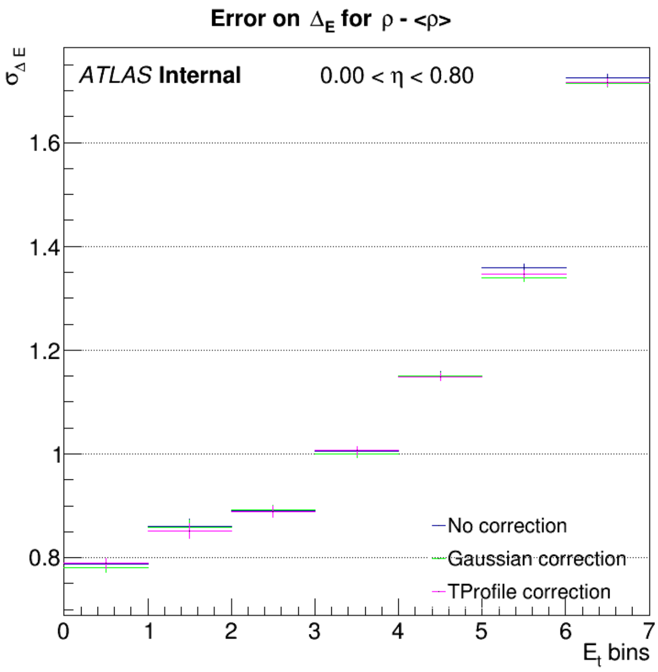

Figure 3: Correction of $\sigma_{\Delta E}$ in the $0 < |\eta| < 0.8$ EMB region using $\rho - < \rho >$. The corrections are negligible at best.

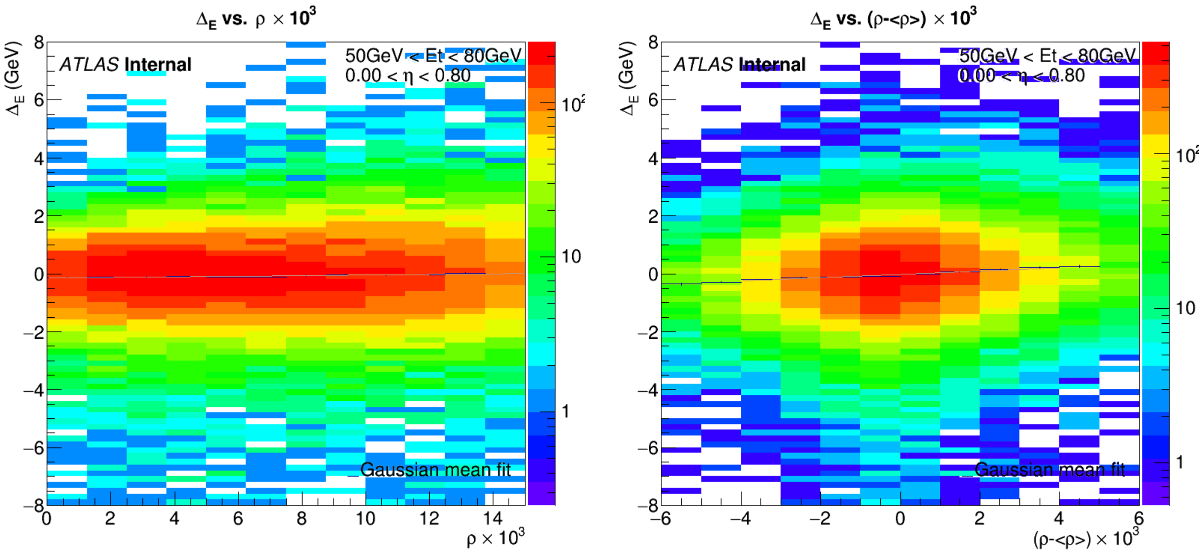

(a) ρ

(b) $\rho - < \rho >$

Figure 4: Dependence on ΔE using ρ with Gaussian mean fit superimposed for $50GeV < E_t < 80GeV, 0 < |\eta| < 0.8$. Note the very weak slope compared to the total dispersion.

6 Conclusion

In this note, the response to pile-up of the EMCal on the energy resolution was studied for μ up to 60. The pileup noise is found to be similar to the previous sliding window clustering algorithm, and displays a dependence on the η region and E_t of the EMCal event, as expected. In $0 < |\eta| < 0.8$ and $15 < E_t < 20$, σ_{noise} is $76 \pm 4GeV$, while for $80 < E_t < 120$ it is $103 \pm 3GeV$. For the same E_t but in $1.6 < |\eta| < 1.82$, the values are $86 \pm 4GeV$ and $120 \pm 3GeV$.

Possible corrections to the pileup noise on the energy resolution are also explored, using ambient energy density, pileup track number, and pileup track energy, as well as two methods for finding correlations. No significant improvement to the resolution was found after corrections due to small correlations.

References

[1] F. Gianotti et al., *Physics potential and experimental challenges of the LHC luminosity upgrade*, The European Physical Journal C-Particles and Fields **39** (2005) 293.

[2] G. Aad et al., *Electron and photon energy calibration with the ATLAS detector using LHC Run 1 data*, The European Physical Journal C **74** (2014) 3071.

[3] *Expected electron and photon energy calibration performance with the ATLAS detector using Super-Clusters*, 2017, URL: https://atlas.web.cern.ch/Atlas/GROUPS/PHYSICS/PLOTS/EGAM-2017-001/ (visited on 09/06/2017).

Appendix

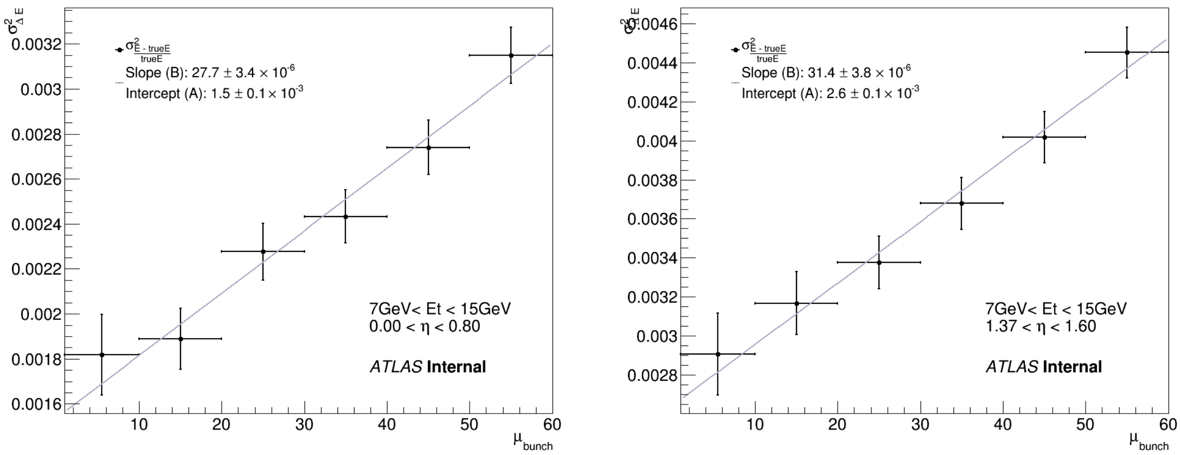

(a) 1st E_t bin, 1st η bin

(b) 1th E_t bin, 3rd η bin

Figure 5: Dependence of the energy resolution on μ

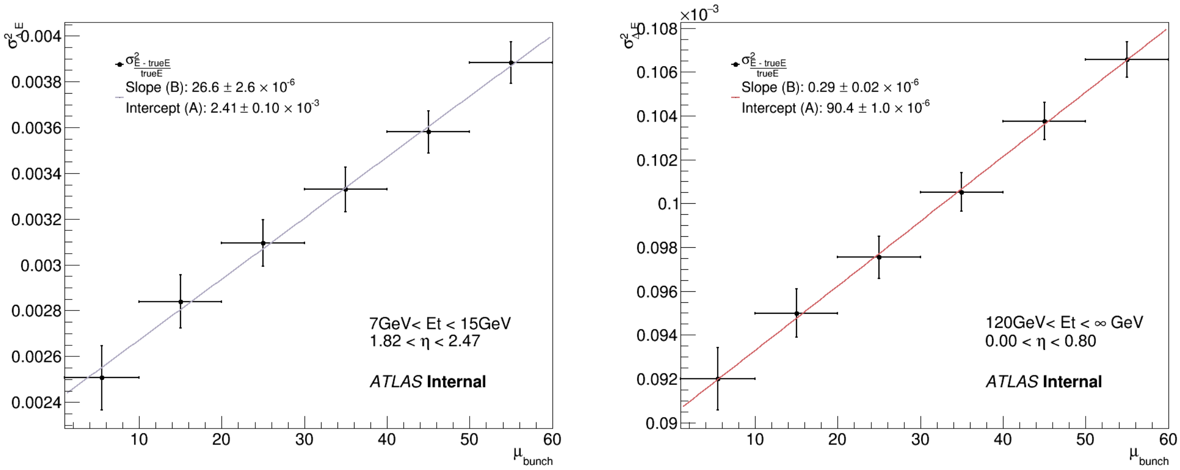

(a) 1st E_t bin, 5th η bin

(b) 7th E_t bin, 1st η bin

Figure 6: Dependence of the energy resolution on μ

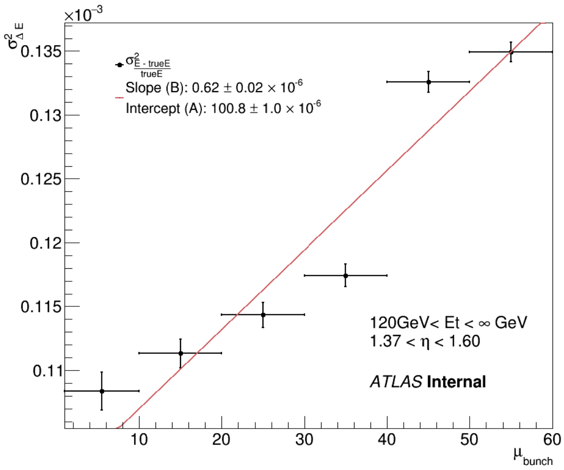

(a) 7th E_t bin, 3rd η bin

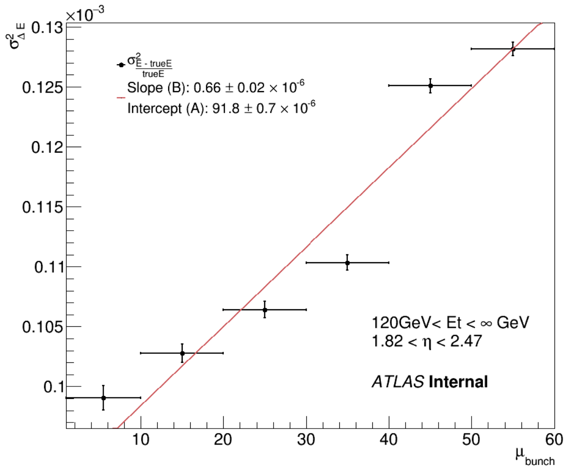

(b) 7th E_t bin, 5th η bin

Figure 7: Dependence of the energy resolution on μ

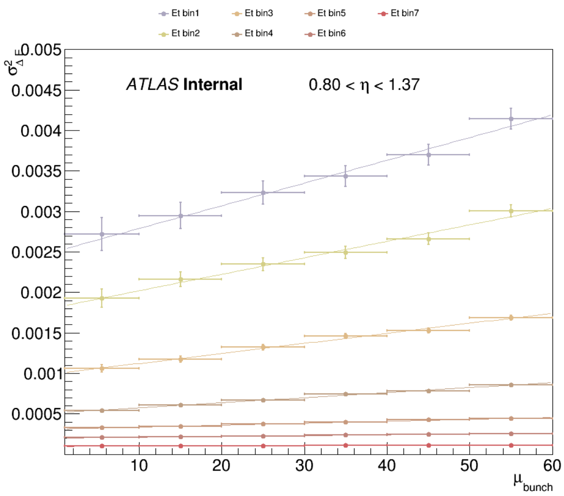

(a) 2nd η bin

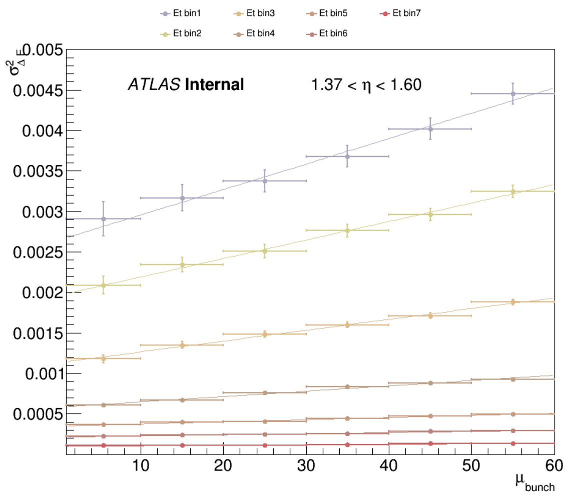

(b) 3rd η bin

Figure 8: Dependence of the energy resolution on μ for all E_t bins, 2nd and 3rd η bin

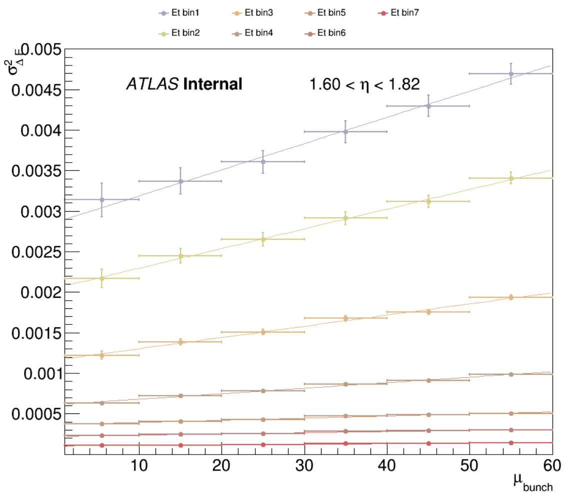

(a) 4th η bin

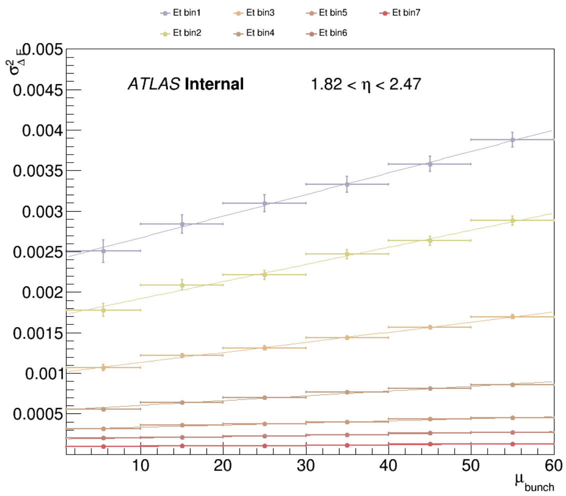

(b) 5th η bin

Figure 9: Dependence of the energy resolution on μ for all E_t bins, 4th and 5th η bin

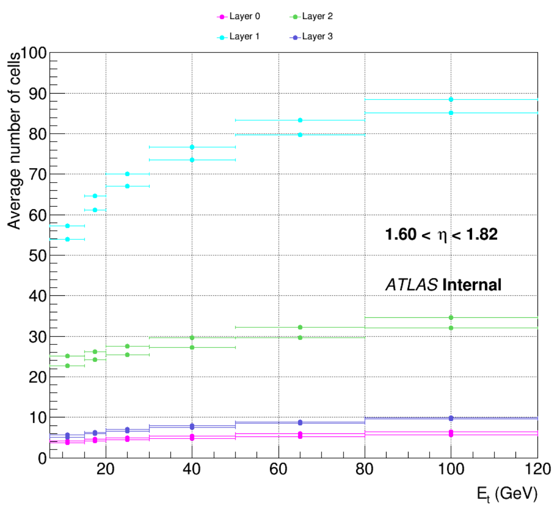

(a) 4th η bin

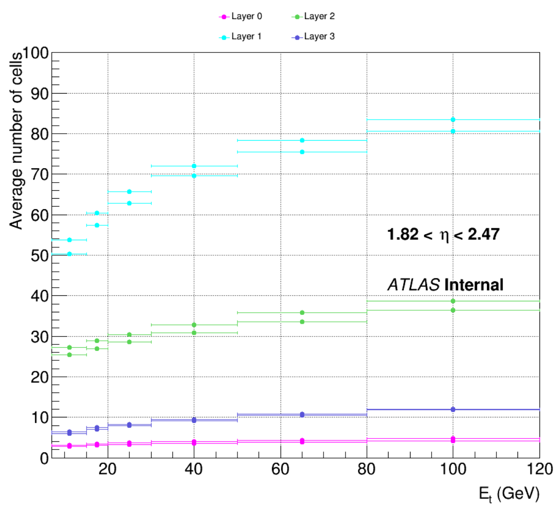

(b) 5th η bin

Figure 10: Average number of cells of supercluster for every layer and every E_t bins, 4th and 5th η bin

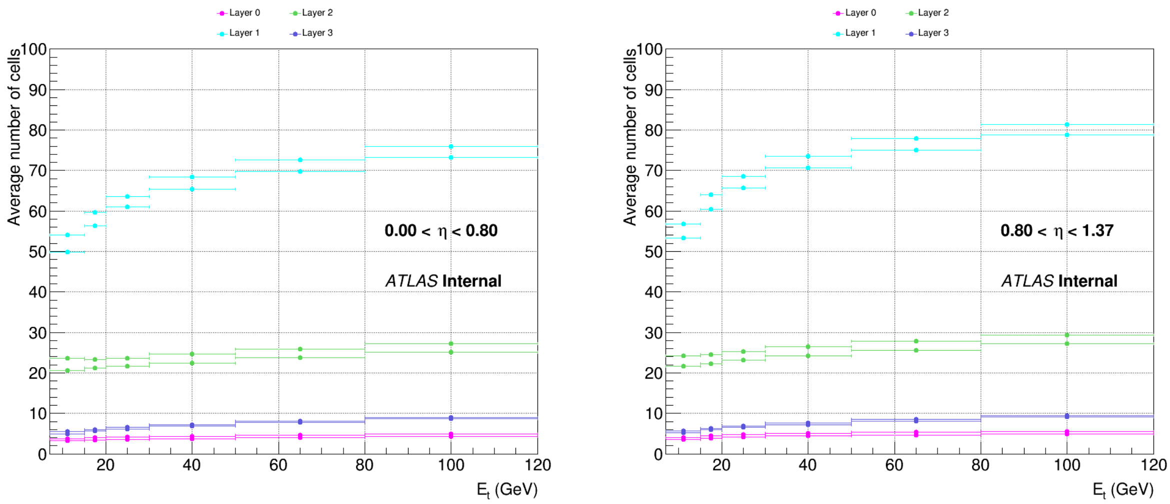

(a) 1st η bin (b) 2nd η bin

Figure 11: Average number of cells of supercluster for every layer and every E_t bins, 1st and 2nd η bin

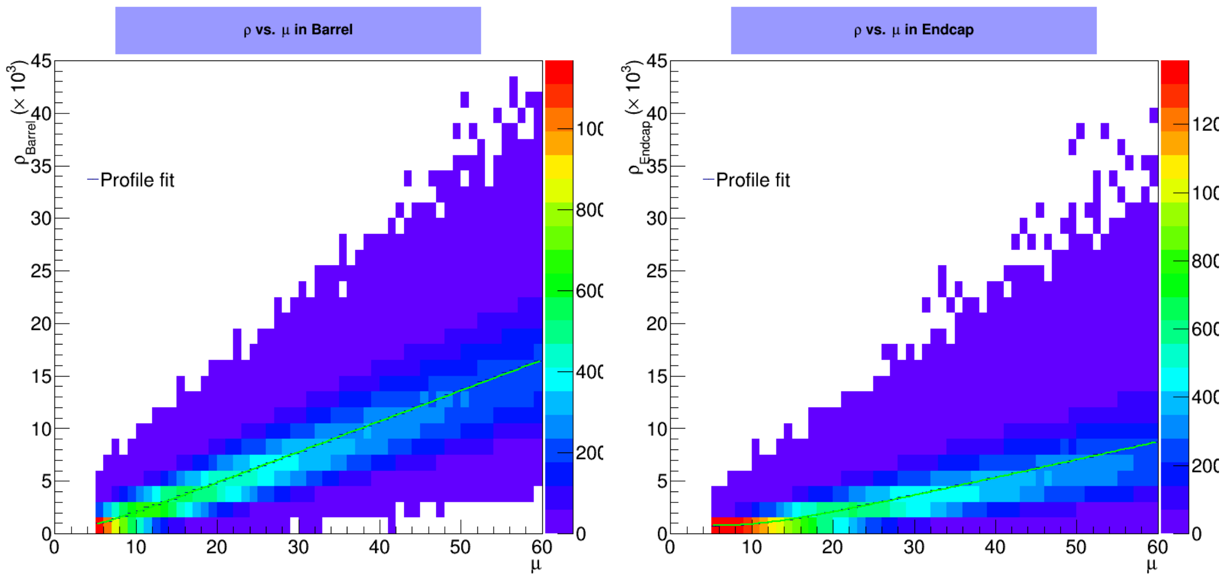

(a) EM Barrel (b) EM End Cap

Figure 12: Dependence of ρ on μ.

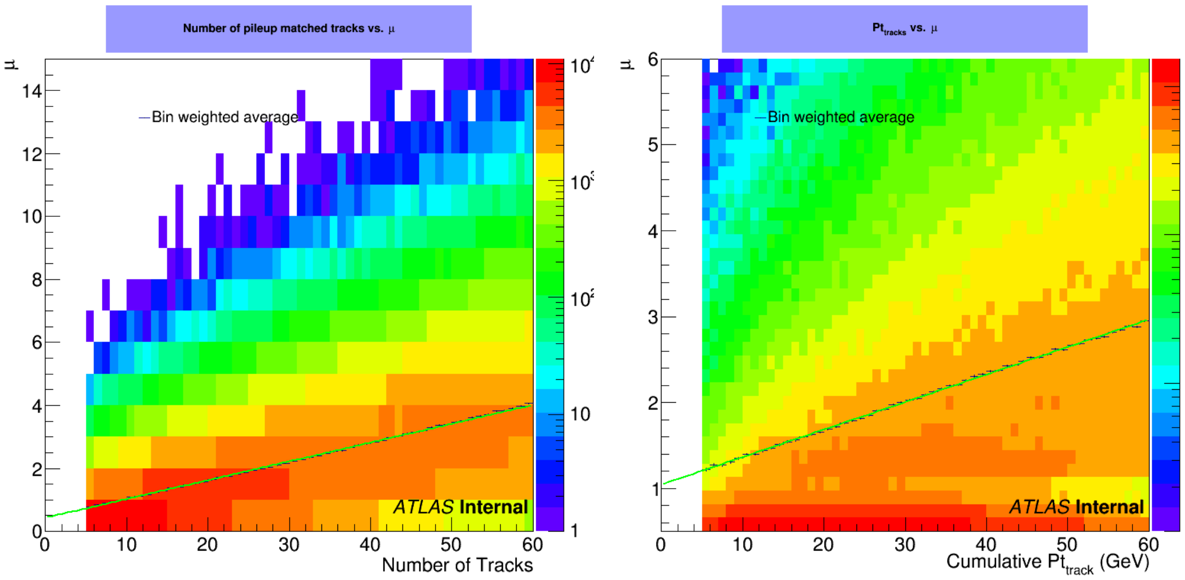

(a) n_{tracks} (b) Pt_{tracks}

Figure 13: Dependence of n_{tracks} and Pt_{tracks} on μ.

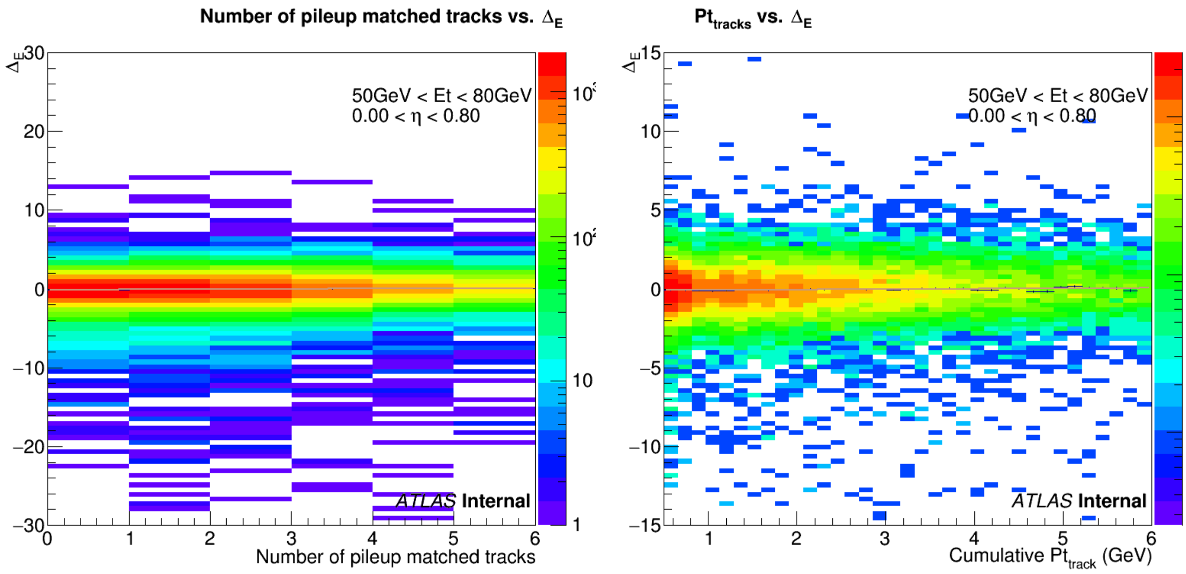

(a) n_{tracks} (b) Pt_{tracks}

Figure 14: Dependence on ΔE using n_{tracks} and Pt_{tracks}

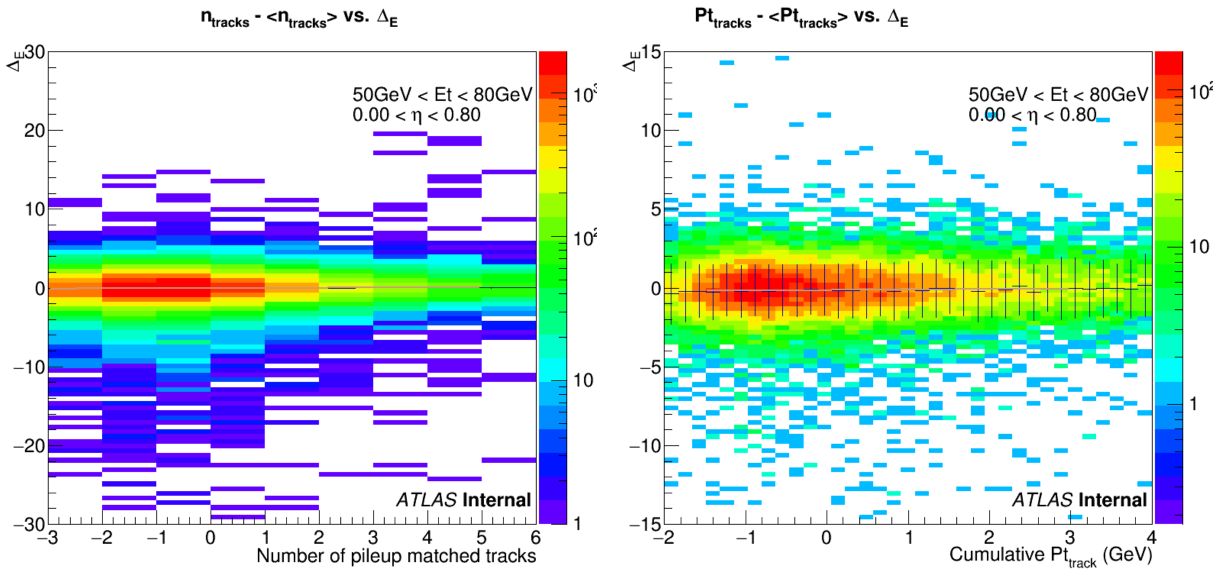

(a) $n_{tracks} - < n_{tracks} >$ (b) $Pt_{tracks} - < Pt_{tracks} >$

Figure 15: Dependence on ΔE using $n_{tracks} - < n_{tracks} >$ and $Pt_{tracks} - < Pt_{tracks} >$

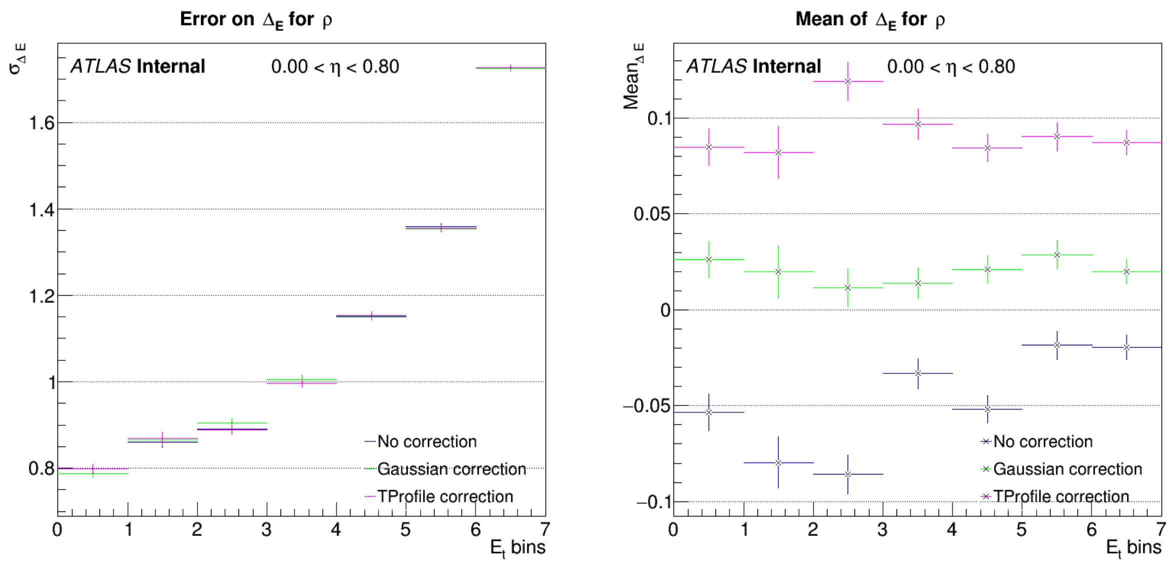

(a) The corrections to $\sigma_{\Delta E}$ are insignificant at best.

(b) Using a weighted average of ΔE typically yields an over-correction. The Gaussian mean gives the expected means around 0.

Figure 16: Correction of $\sigma_{\Delta E}$ and $< \Delta E >$ in the $0.0 < |\eta| < 0.8$ EMB region, using ρ.

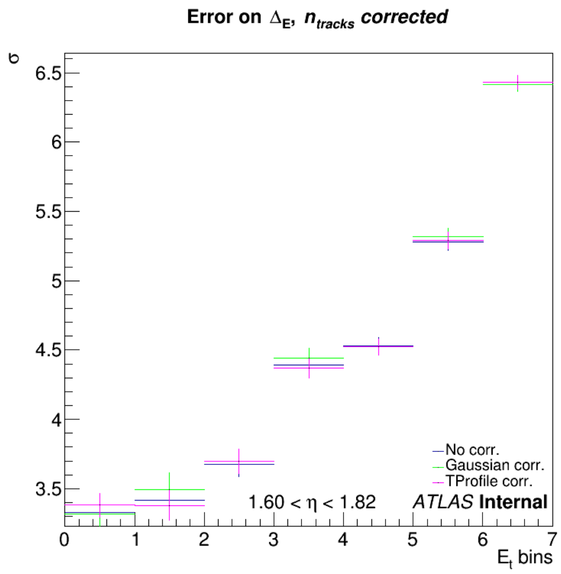

(a) The corrections to $\sigma_{\Delta E}$ are insignificant at best.

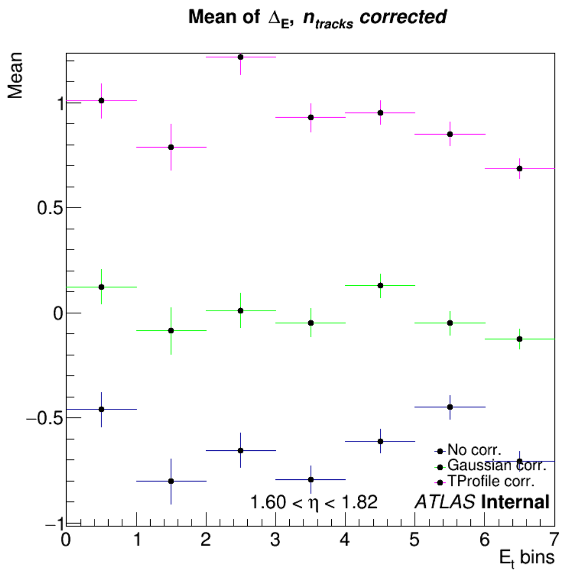

(b) Using a weighted average of ΔE typically yields an over-correction. The Gaussian mean gives the expected means around 0.

Figure 17: Correction of $\sigma_{\Delta E}$ and $< \Delta E >$ in the $1.6 < |\eta| < 1.82$ EMEC region, using n_{tracks}. Here, similar scenario as above is seen.

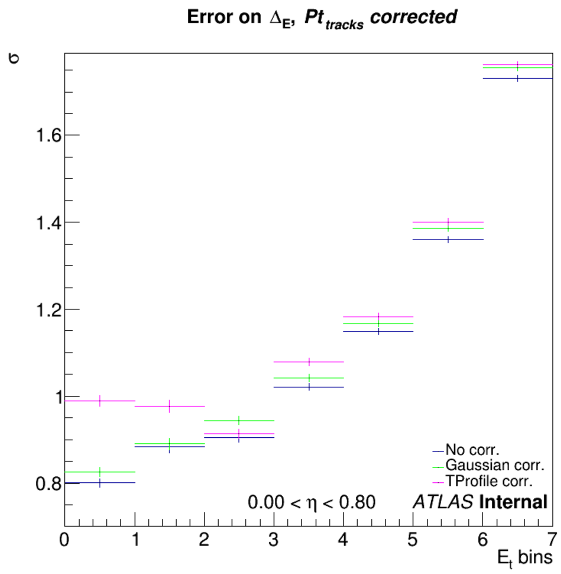

(a) Pt_{tracks}

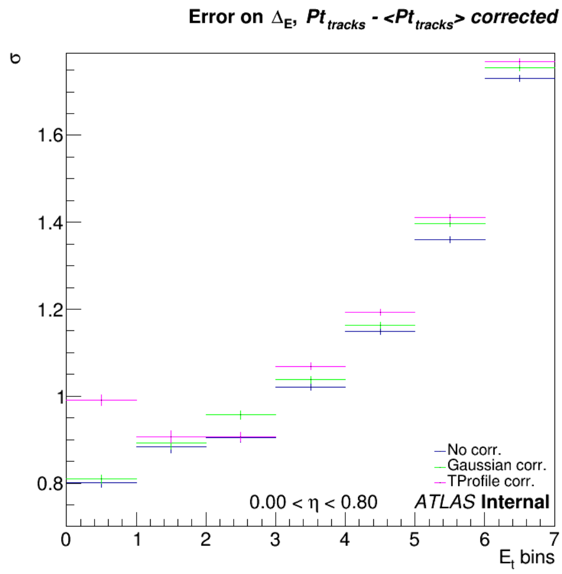

(b) $Pt_{tracks}- < Pt_{tracks} >$

Figure 18: Correction of $\sigma_{\Delta E}$ and $< \Delta E >$ in the $0.0 < |\eta| < 0.80$ EMB region, using Pt_{tracks}. The corrections are significantly worse here.